BL25SU
Soft X-ray Spectroscopy of Solid

1. Introduction

BL25SU is utilized for soft X-ray spectroscopic studies on electronic/magnetic states and surface structures of condensed matter. The beamline consists of two branch lines. The A-branch is specialized for high-energy-resolution X-rays suitable for electron spectroscopy experiments, whereas the B-branch is optimized for a high photon flux beam with a small angle divergence [1-3] and is mainly used for X-ray magnetic circular dichroism (XMCD) experiments.

The main topics related to the beamline apparatuses in FY2024 are as follows: i) the establishment of a method for the crystal-axis determination of single crystals for soft X-ray spectroscopy, ii) the installation of an alkali metal deposition system for angle-resolved photoemission spectroscopy (ARPES), and iii) the installation of a silicon drift detector (SDD) for partial fluorescence yield (PFY) X-ray absorption spectroscopy in XMCD experiments.

2. Experimental stations in the A-branch

2-1. Spectroscopic low-energy electron microscope (SPELEEM) (First station)

The SPELEEM apparatus (LEEM III with an energy analyzer, ELMITEC GmbH), originally operated at BL17SU [4] and later relocated to BL25SU, began user operation in the 2022B term. The measurement software was substantially modified to control the BL25SU optics. With this software, sequential measurements under various conditions, including XAS, chemical mapping, XMCD, and X-ray photoemission spectroscopy, are now available. For XMCD, PEEM images can be obtained using a 0.1 Hz circularly polarized switching system.

2-2. Retarding field analyzer (RFA) (Second station)

Photoelectron holography is applicable to studies of local structures with multiple chemical states [5]. This method requires wide-range photoelectron angular distribution patterns with sufficiently high energy resolution to resolve chemical shifts in inner-core levels. A display-type RFA with an energy resolution ($E/\Delta E$) of up to 2000 is currently in operation for such measurements [6]. Using this apparatus, dopant sites in BiS_2-based superconductors [7] and the arrangement of interfacial defects in the oxide layer of diamond

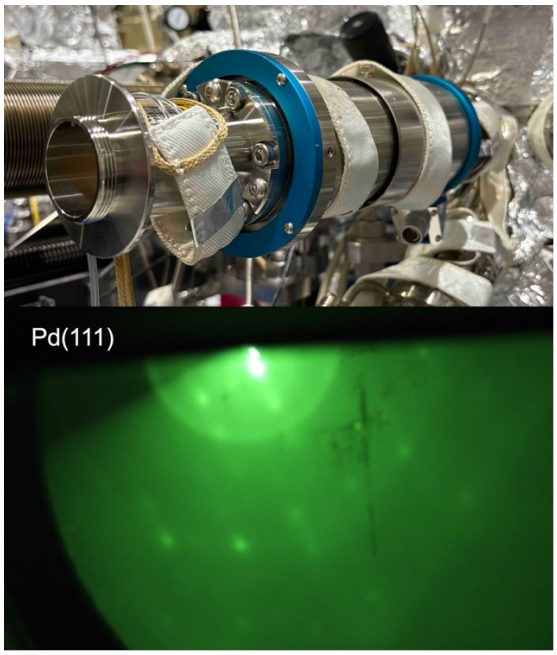

Fig. 1. Photograph of the RHEED system (upper) and the RHEED pattern of a Pd (111) substrate (lower).

semiconductors [8] have been determined.

In FY2022, a sample manipulator with cooling capability was installed, enabling photoelectron holography experiments below 6 K. In FY2023, a left–right circular polarization measurement program connected to the 0.1 Hz kicker system was developed, achieving low-noise, high-yield holography images. In FY2024, the reflection high-energy electron diffraction (RHEED) system was upgraded (Fig. 1), simplifying the electron gun operation and enabling the efficient *in situ* monitoring of sample surface conditions during preparation.

2-3. Microbeam ARPES (Third station)

The ability to select flatly cleaved areas, often microscopic in size, from poorly cleaved sample surfaces is valuable for ARPES [9]. To enhance this capability, a micro-ARPES end-station equipped with a Scienta Omicron DA30 analyzer and a micro-focusing mirror was developed [10, 11]. The typical focusing size is 0.4 μm (vertical) × 10 μm (horizontal), and the beam spot on the sample surface is as small as 10 μm even at a glancing angle of 5 degrees. This end-station has been available for public use since FY2018.

In FY2022, an automatic real-space scanning program was implemented using LabVIEW software. In FY2023, an automatic program for incident-photon-energy–dependent measurements was developed with Python and AutoHotkey to investigate the electronic structure along the k_z momentum (perpendicular to the sample surface). In addition, a soft X-ray absorption measurement program in the total electron yield mode was created with Python to support resonant photoemission spectroscopy. This program also enables users to analyze chemical states in microscale real space from XAS spectra.

In FY2024, to mitigate sample charging effects caused by high flux in low-conductivity materials, a potassium deposition source was installed in the preparation chamber. Potassium was chosen because electron doping can be induced at the surface, thereby improving conductivity. Consequently, users can also investigate the carrier-level dependence of electronic states by tuning the Fermi level.

3. Experimental stations in the B-branch

3-1. Renewal of standard samples for incident photon energy calibration at B-branch

The B-branch is mainly used for XMCD experiments. In this branch, energy calibration has been performed using the X-ray absorptions of $CaCO_3$, MnO, $Sr_3Fe_5O_{12}$, CuO, Gd_2O_3, and SiO_2 powders. To improve the accuracy of the calibration curve in the higher photon energy region (>1,000 eV), Al_2O_3 and P_3O_5 powders were newly introduced.

3-2. X-ray magnetic circular dichroism (XMCD)

The electromagnet-type XMCD is a versatile apparatus that provides various experimental conditions. Its manipulator can accommodate three types of sample holder: for low-temperature measurements, for high-temperature measurements, and for measurements under electric fields or current flow. The signal detection method can also be selected from among the total electron yield (TEY) and transmission modes. A high-precision manipulator, introduced in FY2020, allows measurements of microscopic areas.

In FY2022, to cope with the recent surge in

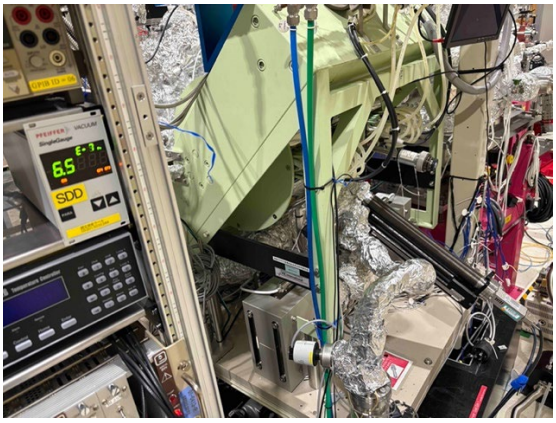

Fig. 2. Photograph of the silicon drift detector (SDD) system.

helium prices, manipulator cooling with liquid nitrogen was tested. As a result, although operation at the fully cooled temperature (77 K) was achieved, stable control at specific intermediate temperatures was not successful owing to insufficient heater output. Further improvements are currently under consideration.

In FY2024, to investigate the detection depth dependence of the magnetic state, an SDD detector was installed (Fig. 2). Because of the extended baking of the special SDD chamber, fluorescence signals can now be detected under ultrahigh-vacuum conditions (8.0×10^{-8} Pa) comparable to those in the TEY mode during experiments.

YAMAGAMI Kohei, NAKAMURA Tetsuro, and KAWAMURA Naomi
Spectroscopy & Imaging Division, JASRI

References:

[1] Nakamura, T. et al. (2014). *SPring-8 INFORMATION* **19**, 102–105.
[2] Nakamura, T. et al. (2015). *SPring-8/SACLA Research Report* **3**(1), 186–200.
[3] Senba, Y. et al. (2016). *AIP Conference Proceedings* **1741**, 030044.
[4] Guo F. Z. et al. (2007). *Rev. Sci. Instrum.* **78**, 066107.
[5] Tsutsui, K. et al. (2017). *Nano Lett.* **17**, 7533.
[6] Muro, T. et al. (2017). *Rev. Sci. Instrum.* **88**, 123106.
[7] Li, Y. et al. (2022). *J. Phys. Soc. Jpn.* **91**, 054602.
[8] Fujii, N. M. et al. (2023). *Nano Lett.* **23**, 1189−1194.
[9] Fujiwara, H. et al. (2015). *J. Synchrotron Rad.* **22**, 776.
[10] Senba, Y. et al. (2020). *J. Synchrotron Rad.* **27**, 1103 (2020).
[11] Muro, T. et al. (2021). *J. Synchrotron Rad.* **28**, 1631.